Journal of the European Ceramic Society **10** (1992) 51–57

Development of Microstructure during Pressureless Sintering of Alumina

P. Quirmbach, M. Wolf, R. J. Brook

Max-Planck-Institut für Metallforschung, Institut für Werkstoffwissenschaft, Pulvermetallurgisches Laboratorium, 7000 Stuttgart 80, FRG

&

H.-W. Hennicke

Technische Universität Clausthal, Institut für Nichtmetallische Werkstoffe, Lehrstuhl für Keramik und Email, 3392 Clausthal-Zellerfeld, FRG

(Received 21 June 1991; revised version received 25 October 1991; accepted 4 November 1991)

Abstract

This paper deals with the evolution, during sintering, of crack-initiating defects in slipcast alumina. The microstructures are characterized by optical microscopy and by SEM, the mechanical behaviour being investigated in four-point bend.

After initial-stage sintering (65–70% t.d.), the samples have defects both in the bulk and at the surface. Increased densification (75–85% t.d.) leads to microstructures where surface defects are predominant sources for crack initiation. Weibull analysis suggests that the minimum strength of the samples increases during densification but that the width of the strength distribution remains constant. The initial flaw distribution thus retains its importance up to at least 85% t.d.

In dieser Arbeit wird die Entwicklung bruchauslösender Defekte beim Sintern schlickergegossener Al_2O_3-Keramiken untersucht. Die Gefügecharakterisierung erfolgte mittels licht- und rasterelektronenmikroskopischer Untersuchungen, das Versagensverhalten wurde mit Vier-Punkt-Biegeversuchen bestimmt.

Im Bereich des Anfangsstadiums des Sinterns (65–70% t.D.) wiesen die Probekörper sowohl Oberflächen- als such Volumenfehler als bruchauslösende Defekte auf. Eine zunehmende Verdichtung des Gefüges (75–85% t.D.) führte dazu, daß ausschließlich Oberflächenfehler bruchauslösend waren. Berechnungen mit Hilfe der Weibull-Statistik wiesen eine Zunahme des unteren Festigkeitswerts der Probenkörper bei gleichzeitigem Anstieg des Dichtegrades nach. Dabei blieb die Streuung der Festigkeitsverteilung konstant. Der Einfluß der Ausgangsfehlerverteilung auf die Festigkeitsverteilung blieb bis zur gemessenen Dichte von 85% t.D. erhalten.

Cet article traite de l'évolution durant le frittage de défauts provoqués par des fissures dans de l'alumine coulée en barbotine. Les microstructures ont été caractérisées par microscopie optique et par SEM, et le comportement mécanique a été étudié par flexion quatre points. Aprés le stade initial du frittage (65–70% t.d.), les échantillons présentent des défauts à la fois à l'intérieur et à la surface. Une augmentation de la densité (75–85% t.d.) conduit à des microstructures dans lesquelles les défauts de surface sont des sources prépondérantes pour l'initiation de fissures. L'analyse Weibull suggère que le minimum de la résistance mécanique des échantillons augmente au cours de la densification, mais que la largeur de la distribution de la résistance mécanique reste constante. Ainsi la distribution initiale des fissures conserve son importance jusqu'à au moins 85% t.d.

Introduction

The mechanical strength of a ceramic component is determined by the existence of flaws or microstructural inhomogenities within the structure. It is therefore important to understand the origin of such

Journal of the European Ceramic Society 0955-2219/92/$05.00

flaws and to correlate this with processing parameters. In this paper, the defects that arise during the evolution of the microstructure at different stages of sintering in a slipcast alumina are characterized.

Earlier studies of microstructure development in specimens of increasing density, starting with the green density, ρ_g, have predominantly dealt with the relationship between grains and pore during sintering[1-7] or have considered the influence of agglomerates.[8-11]

The purpose here is to measure mechanical strength at several different density levels during densification to explore the development of the strength-determining defects. Major issues are the extent to which defects become more severe or less severe (healing) during processing and the extent to which the size range of defects changes during sintering. This behaviour is recorded by the Weibull modulus m at each density stage.

2 Experimental Procedure

2.1 Slip preparation

The slip consisted of an alumina powder (A16-SG, Alcoa, Pittsburgh, USA), a deflocculant (CE 64, Zschimmer & Schwarz, Lahnstein, FRG) and a pH-regulating ingredient (triethylamine p.a. $\geq 99{\cdot}5\%$, Fluka, Buchs, Switzerland). The process of slip casting followed the path shown in Fig. 1. Additionally, the solids content was fixed at 70 wt%. Determination of the zeta-potential of the powder was made by conducting experiment based on electrophoresis (Zetasizer IIc, Malvern, Worcestershire, UK). The best working range was found to be around pH ≈ 10 when triethylamine was used to control the basicity. The quantity of deflocculant was varied between 0 and 4 wt%. All samples, when measured by rotating viscosimeter, showed Bingham viscous behaviour.[12] With the addition of 0·3 wt% CE 64 to the powder mass the slurry showed the lowest viscosity.

2.2 Cast preparation and the forming of green bodies

The plaster form was protected by exposing it for 180 s to a solution of alginate (ammonium alginate, Roth, Karlsruhe, FRG) just before slip casting. The inner surface of the plaster form was thus covered with a thin microporous skin. This membrane then retained fine solid grains, but was permeable to the dispersant. Additionally, the skin of alginate improved the later separation of the samples from the mould; any adhering alginate burned out during sintering. After 2 h, the green bodies were removed from the plaster form, then dried for 24 h in air and finally for a similar time in a drying chamber at 80°C. Subsequently, the green density was determined by the Archimedes method; the immersion medium was water, the sample being protected by a permeable water-insoluble layer. A value of $\rho_g = 57{\cdot}0 \pm 0{\cdot}1\%$ of the theoretical fully dense value was found for all samples.

The green bodies received no machining or surface finishing before sintering, in order to avoid any defects that might be caused by such treatments.

2.3 Sintering process

Confirmation that the different density stages had been achieved was made by the Archimedes method. The sintering schedule is shown in Fig. 2, together

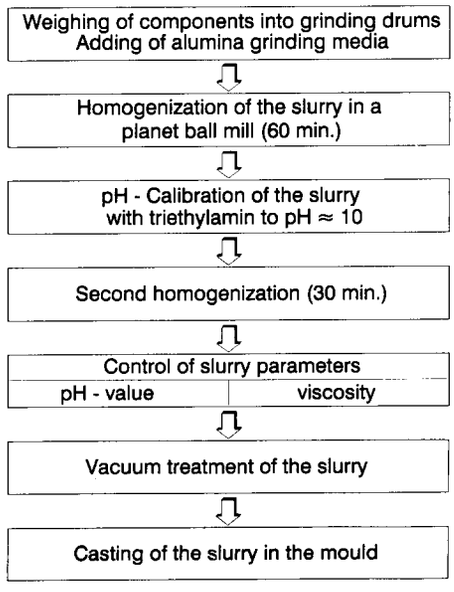

Fig. 1. Flow chart of slurry preparation.

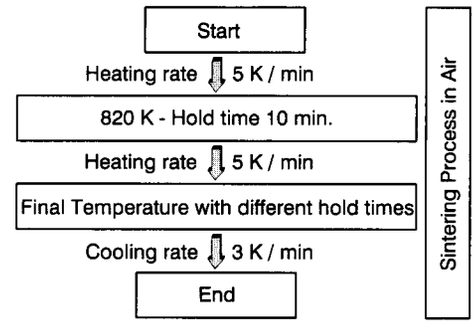

Step	Final Temperature	Hold Time	Density	Linear Elongation
Unit	K	min.	% t.d.	ΔL / Lo
1	1500	90	64.7±0.1	-4
2	1600	15	70.5±0.5	-6
3	1600	110	75.1±0.5	-8
4	1650	105	80.0±0.2	-10
5	1700	35	84.4±0.3	-12

Fig. 2. Sinter program with results.

with a listing of the hold times and temperatures needed to reach the target density values.

The measured linear elongations given in the table, when combined with the measured density changes, suggest that shrinkage occurred isotropically.

2.4 Four-point bend tests

This form of strength test was preferred to increase the effective test volume.[13] The problem in using samples with unpolished surfaces is that surface irregularities can initiate stress concentrations at the supports. For this reason, samples failing at the supports are not included in the reported data.

The specimens were loaded at constant strain rate ($0{\cdot}5\,mm\,s^{-1}$) in a 40/20 mm support arrangement (Hydropuls PSA Schenck, Darmstadt, FRG). The high strain rate was chosen to avoid subcritical crack growth during the experiments.

2.5 Micrography

The external surfaces and fracture surfaces were examined by scanning micrography (Stereoscan 200, Cambridge Instruments, Cambridge, UK) and by optical microscopy (M 8, Wild, Heerbrugg, Switzerland).

3 Results

3.1 Microscopical characterization of specimen surfaces and crack surfaces

3.1.1 Specimen surfaces

The specimen surfaces reflect the different degrees of densification in showing a progressive evolution of the surface topography. A decrease in surface roughness is apparent. The coarse furrows, that can be seen on the surfaces of the Step 1 samples (65% t.d.) as shown in Fig. 3, change into small wave-like features by the time Step 5 (85% t.d.) is reached in Fig. 4.

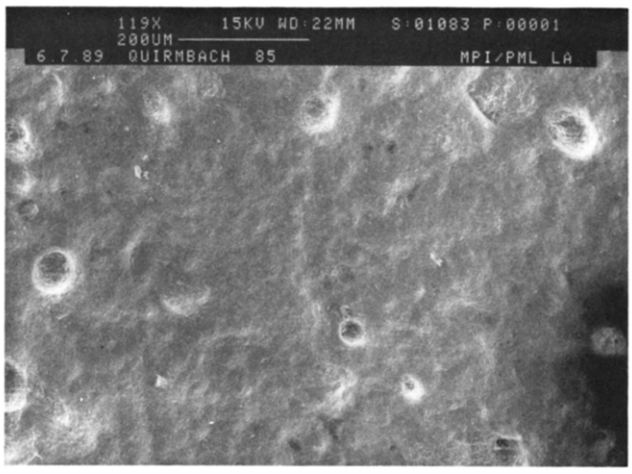

Fig. 3. Surface of Step 1 sample.

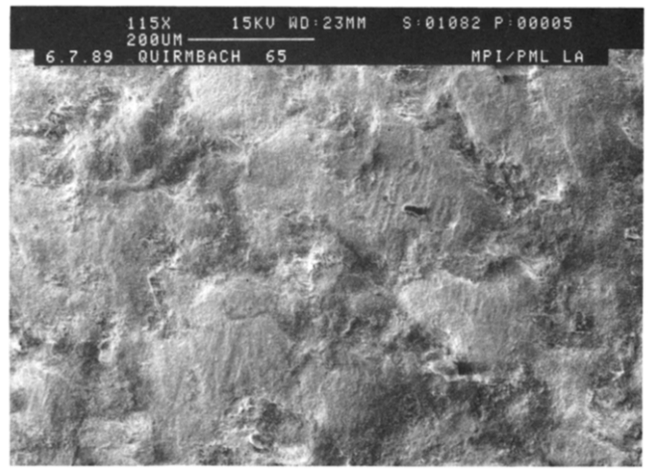

Fig. 4. Surface of Step 5 sample.

The surfaces of specimens after Step 1 reveal no large-scale (i.e. 50 μm) features, whereas those from Step 5 specimens show cratering. These depressions are hemispherical with diameters of some 60–100 μm.

3.1.2 Crack surfaces

Fine pores cover the crack surface of the specimen after the treatment corresponding to Step 1 (Fig. 5). The quantity and size of the pores increase towards the surface, where the pore size reaches 5–10 μm. These large pores occur mainly within the first 60 μm from the specimen surface.

In contrast, samples examined after Step 5 show large pores or cavities with a size of 60–100 μm at the specimen surface only (Fig. 6). No large pores in the subsurface region were observed.

3.2 The characterization of crack-initiating defects

After the mechanical tests, the defect type responsible for fracture origin on the fracture surfaces was

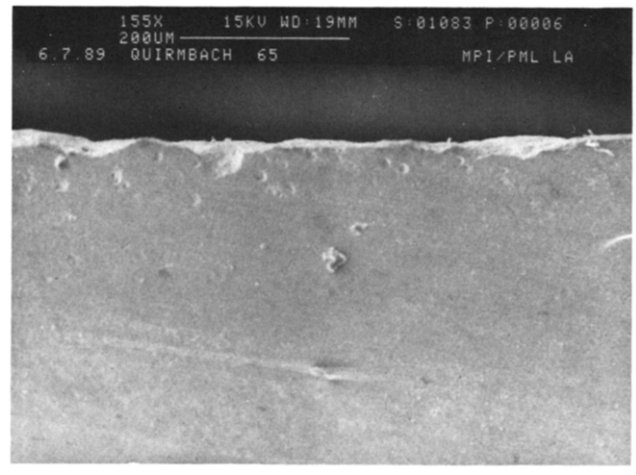

Fig. 5. Crack surface of Step 1 sample.

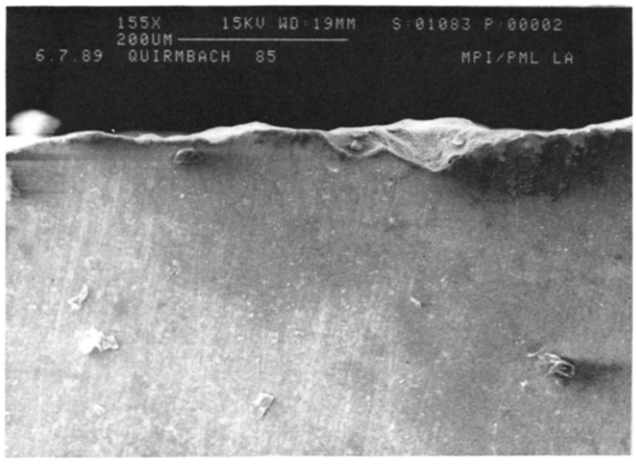

Fig. 6. Crack surface of Step 5 sample.

identified and both bulk (Fig. 7) and surface defects (Fig. 8) were found. The critical defects were in all cases pores.

Optical evaluation of all fracture surfaces showed that the fraction of samples for which bulk defects were responsible for fracture rapidly decreased on progressing through the five sintering steps (Fig. 9). In samples with 80–85% theoretical density,

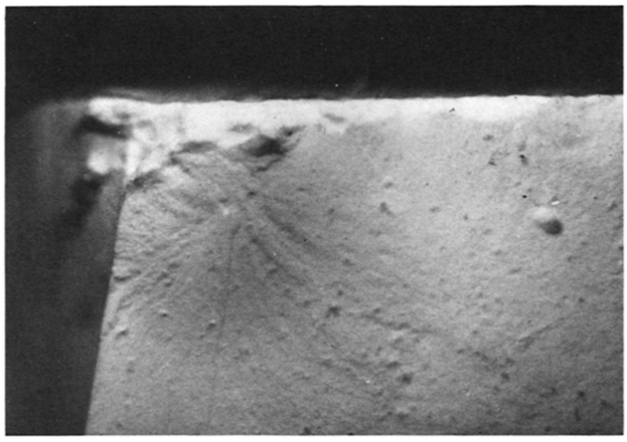

Fig. 7. Volume (bulk) defect. Magnification: 25×.

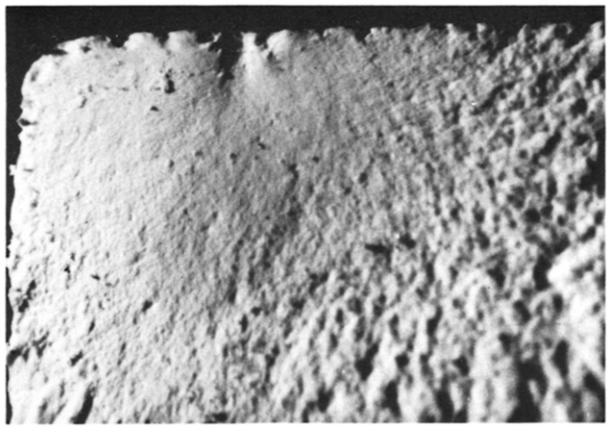

Fig. 8. Surface defect. Magnification: 25×.

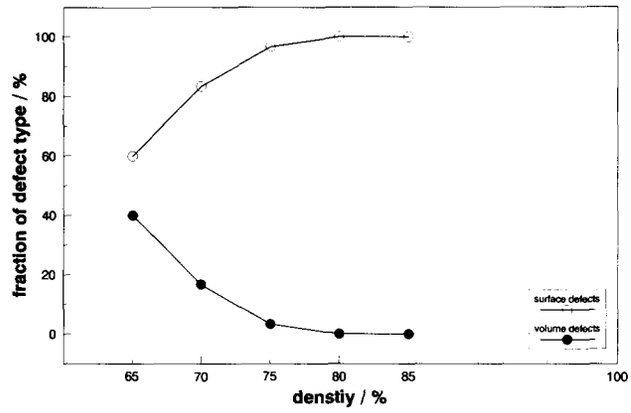

Fig. 9. Change in defect type.

only surface defects were active as crack-originating flaws.

3.3 Weibull statistics

The Weibull procedure treats the fracture probability, F, based on a weakest-link theory, while assuming a homogeneous stress field, Σ.[14] This implies that a given defect has the same critical stress, σ_c, for failure, wherever it occurs in the sample. At the critical stress, the defect initiates the failure of the whole body.[15]

The use of Weibull statistics requires some 30 single strength values, which are then analysed in terms of the Weibull distribution function:

$$F = 1 - \exp\left\{-V\left(\frac{\sigma - \sigma_u}{\sigma_o}\right)^m\right\} \qquad (1)$$

where:

F = fracture probability
σ = stress
σ_u = threshold stress
σ_o = material specific constant (scaling parameter)
V = stressed volume
m = Weibull modulus

The graphical representation commonly assumes

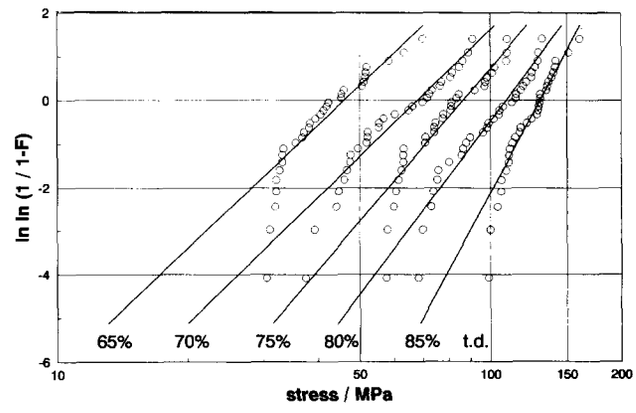

Fig. 10. Weibull plots calculated using the two-parameter distribution.

$\sigma_u = 0$ and shows the relation between measured stress plotted as $\ln \sigma$ and the fracture probability plotted as $\ln \ln F$. The slope of such a graph then represents the Weibull modulus m. In this work, the slope is determined from the data by the maximum-likelihood method.[16] With the assumption as in Fig. 10 that $\sigma_u = 0$, eqn (1) represents the two-parameter Weibull distribution.

However, the form of the data in Fig. 10 suggests a threshold stress value of $\sigma_u \neq 0$ for every density stage. Taking the indicated values for σ_u and plotting the data according to the three-parameter distribution (eqn (1) $\ln \ln F$ versus $\ln(\sigma - \sigma_u)$) the data shift as represented by the example of 65% density sample in Fig. 11.

Comparison of the two- and three-parameter evaluations makes it apparent (Fig. 12) that the three-parameter distribution gives a better fit to the data.

The evolution of the reliability in the progressively more sintered microstructures can be expressed in terms of changes in the Weibull modulus m. Figure 13 shows apparent steady improvements in the Weibull moduli using the two-parameter evaluation,

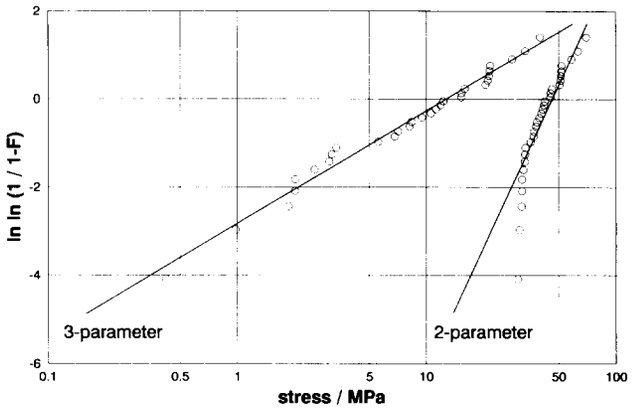

Fig. 11. Two-parameter–three-parameter comparison of Weibull modulus for the Step 1 sample; the stress axis is in terms of σ and $(\sigma - \sigma_u)$ for the two distributions respectively.

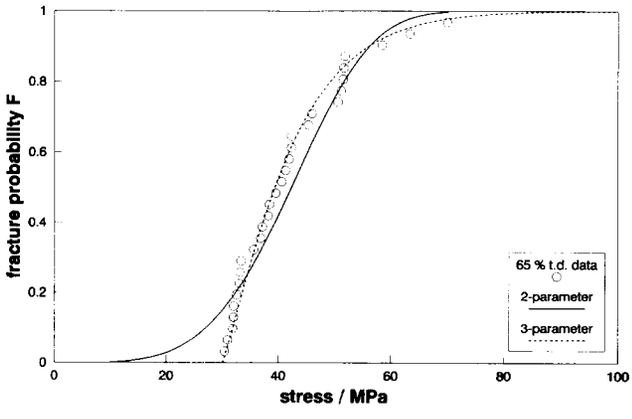

Fig. 12. Step 1 sample fitting.

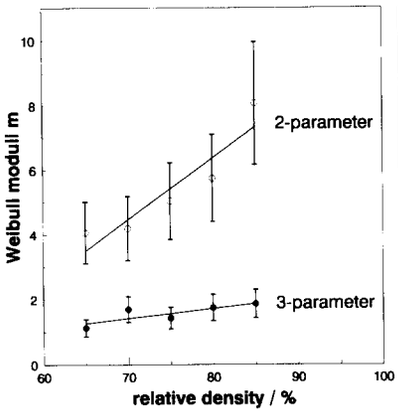

Density	Weibull moduli m	
	2-param.	3-param.
65 %	4.06	1.12
70 %	4.19	1.69
75 %	5.04	1.42
80 %	5.75	1.74
85 %	8.07	1.86

Fig. 13. Weibull moduli m at the different sintering stages.

i.e. higher reliability as higher densities are attained. In contrast, the three-parameter evaluation gives only a small increase in the Weibull moduli with increasing density, suggesting no significant change in reliability. The smaller 90%-confidence limits for the three-parameter evaluation shown in Fig. 13 are further suggestive of the better fit.

It is to be noted that the different increase in the Weibull moduli corresponding to the different evaluation methods is due to a mathematical effect originating from the logarithmic scaling of the Weibull formula (compare to Fig. 11).

For further analysis the respective defect population (i.e. respective pore populations) of the different sintering stages can be described as indicated in Fig. 14 in terms of an exponential law for the distribution of defect lengths:[17]

$$g = g^* \cdot \left(\frac{a}{a_0}\right)^{-r} \tag{2}$$

where:

g = number of defects per unit volume and per length increment
g^* = scaling parameter
a = defect length
a_0 = scaling parameter
r = exponent

and:[17]

$$r = \frac{m}{2} + 1 \tag{3}$$

Plotting the defect populations for the different sintering stages, it can be seen that the slopes shift to lower defect length with increasing densification (Fig. 15). The exponent r of the defect population was calculated in each case with the three-parameter evaluation.

Owing to the lack of a confirmed defect model, Fig. 15 does not show absolute values. However, the

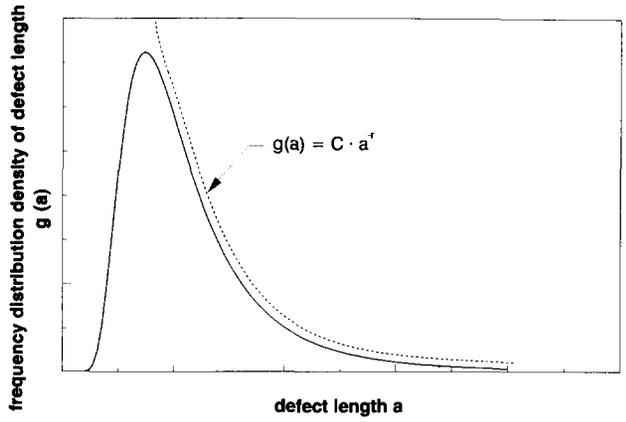

Fig. 14. Schematic defect distribution.

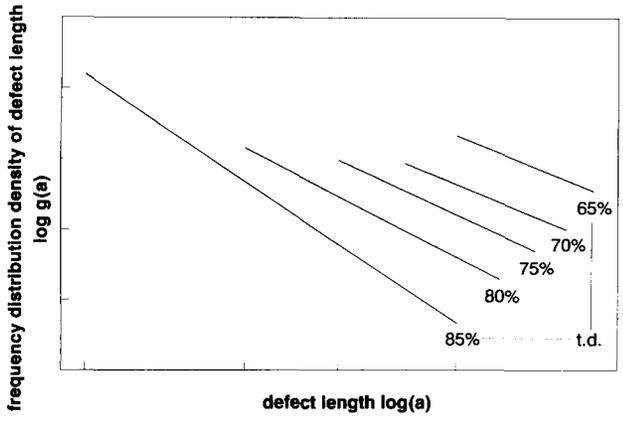

Fig. 15. Populations of defects for different sintering stages.

parallel shift at 65–70% t.d. indicates that there is a proportional shrinkage of the pores. The small change in slope at 75–85% t.d. indicates a change in defect length distribution. The pores as defects change their shrinkage behaviour on reaching the later sintering stage. (In the absence of an adequate defect model to describe the shape of pores, the model of a pore with a circumferential crack has been used for estimating the defect distribution $g(a)$.)

4 Discussion

The samples in the present study are representative of what are commonly considered to be the first two stages of the sintering process, i.e. up to the closed-pore stage at some 93% density. It should be emphasized, however, that homogeneous development of the microstructure can be difficult to achieve and that structures representative of the different stages are commonly found in different regions of a single sample. The most notable fracture in the early stage structure (Fig. 5) is the aggregation of small pores in an area just below the surface (first 60 μm). During the forming process the finer powder particles have a tendency to move with the suspending fluid. The skin formed from the alginate solution prevents the entry of these fine powder particles into the capillaries of the mould. Instead, these build the first layers of the developing green body. A depleted layer consisting of larger particles and agglomerates with larger, inter-agglomerate porosity then accumulates on the growing layers of the cast. Figure 5 shows the microstructure of specimens after removal of water and initial heating.

The surfaces of samples in the initial stage contain no large pores (Fig. 3). The variation of surface topography with progressive sintering is due to the growth of pores located first directly under the surface. At a later stage, the matter bridging these pores collapses and the pores become open surface features (Fig. 4). This type of pore increases in quantity and size throughout the intermediate stage. Analogous behaviour has also been found in hot isostatically pressed specimens.[18]

The mechanical properties of these porous samples as recorded by Weibull statistics reflect mainly the porosity development and not that of grain size. Earlier literature studies have reported comparative tests on green and dense specimens;[19] it has been found that, during densification, only small changes in the determined two-parameter Weibull modulus occurred. This was due to the fact that the defects in the green bodies persisted during sintering, so that they always acted as the crack-initiating defects. No healing effects were obtained.

This work, in contrast, shows that, over the five different steps, the Weibull moduli, as determined with the two-parameter evaluation, increase continuously (Fig. 13). The Weibull moduli as derived with the three-parameter distribution also increase, but not so strongly as in the two-parameter evaluation. This is, as noted, due to logarithmic scaling in Weibull plots.

As seen in Fig. 15, different behaviours for the defect length distributions are obtained. The parallel shift in the low density stages (65%–70% t.d.) represents a proportional shrinkage of the defects. The change in the slope for the next density stages (75%–85% t.d.) indicates an alteration in defect length distribution, perhaps representative of a change in mean pore geometry.

The increasing microstructural reliability is also supported qualitatively by examination of the crack-initiating defects (Fig. 9). The early stage specimens show critical bulk defects (Fig. 7) as well as critical surface defects (Fig. 8). This is best related to the accumulation of pores just below the surface. Later stage samples show only surface defects, the

conversion of bulk into surface defects continuing until the surface structure limits the stability of the component. Such a correlation would suggest the value of strength measurements on partially sintered samples to underline developments in the observed defect population and to indicate the necessary paths for process and component optimization.

References

1. Coble, R. L., Effects of particle-size distribution in initial-stage-sintering. *J. Amer. Ceram. Soc.*, **56** (1973) 461–6.
2. Eadie, R. L., Wilkinson, D. S. & Weatherley, G. C., The rate of shrinkage during the initial-stage of sintering. *Acta Metall.*, **22** (1974) 1185–95.
3. Greskovich, C. & Lay, K. W., Grain growth in very porous Al_2O_3 compacts. *J. Amer. Ceram. Soc.*, **55** (1972) 142–6.
4. Beere, W., The second stage sintering kinetics of powder compacts. *Acta Metall.*, **23** (1975) 139–45.
5. Bruch, C. A., Sintering kinetics for the high density alumina process. *Ceram. Bull.*, **41** 799–806.
6. Yan, M. F., Cannon, R. M., Bowen, H. K. & Chowdry, U., Effect of grain size distribution on sintered density. *Mater. Sci. Eng.*, **60** (1983) 275–81.
7. Venkataraman, K. S., DiMilia, R. A., Predicting the grain-size distributions in high-density, high-purity alumina ceramics. *J. Amer. Ceram. Soc.*, **72** (1989) 33–9.
8. Shaw, N. J. & Brook, R. J., Structure and grain coarsening during the sintering of alumina. *J. Amer. Ceram. Soc.*, **69** (1986) 107–10.
9. Brook, R. J., Pores and grain growth kinetics. *J. Amer. Ceram. Soc.*, **52** (1969) 339–40.
10. Evans, A. G., Considerations of inhomogenity effects in sintering. *J. Amer. Ceram. Soc.*, **65** (1982) 497–501.
11. Lange, F. F., Sinterability of agglomerated powders. *J. Amer. Ceram. Soc.*, **67** (1984) 83–9.
12. Moore, F. & Hennicke, H. W., *Rheologie in der Keramik*. Herrmann Hübener Verlag, Abt. Technischer Verlag, Goslar, 1967.
13. Munz, D., Effect of specimen type on the measured values of fracture toughness of brittle ceramics. In *Fracture Mechanics of Ceramics*. Plenum Press, New York, London, 1983, pp. 1–26.
14. Weibull, W., A statistical distribution function of wide applicability. *J. Appl. Mech.*, **18** (1951) 293–7.
15. Pabst, R. F., Aspekte der modernen Bruchstatistik. *Fortschrittberichte der VDI-Zeitschriften*, **18** (1981) 156–99.
16. DIN 51110, Part 3, Prüfung von keramischen Hochleistungswerkstoffen. 4-Punkt-Biegeversuch bei Raumtemperatur, 1991.
17. Wolf, M., Danzer, R. & Petzow, G., Defekt- und Bruchstatistik von SSiC, *Forschrittberichte der Deutschen Keramischen Gesellschaft*, **6** (1991).
18. Kellet, B. J. & Lange, F. F., Experiments on pore closure during hot isostatic pressing and forging. *J. Amer. Ceram. Soc.*, **71** (1988) 7–12.
19. Kendall, K., McAlford, N. N. & Birchall, J. D., The strength of green bodies. In *British Ceramic Society Proceedings No. 37*, 8th Meeting on Special Ceramics, London, 1985.